ON THE AMOUNT OF INFORMATION CONTENT IN MICROWAVE RADIOMETRY FOR WET DELAY ESTIMATION

J. Gual and A. Camps

Remote Sensing Lab, Dept. of Signal Theory and Communications
Universitat Politècnica de Catalunya-Barcelona Tech and IEEC/CTE-UPC
UPC Campus Nord, building D4, 08034 Barcelona, Spain,
e-mail: jmgualcovas@gmail.com, camps@tsc.upc.edu

***Abstract*—This work aims at determining the set of optimum frequencies to be used in the companion microwave radiometers in future synthetic aperture radar altimeters, to provide higher spatial resolution of the atmospheric water vapor state so as to improve the wet delay correction in coastal regions. The channel selection is based on the study of the frequencies that provide the largest amount of information, as defined by the largest information entropy change from a prior knowledge state. It is found that four frequencies, one close to the 22 GHz peak, and three other ones around 175.188 GHz provide a near optimum compromise between the amount of information measured, and the instrument's complexity.**

***Index Terms*—wet delay, atmospheric water vapor, microwave radiometer, radar altimeter, weighting functions, entropy, information content.**

I. INTRODUCTION

Satellite altimetry plays an important role among the Earth observation techniques, and it is very useful for ocean missions. Coastal Altimetry (approximately 0-50 km away from the coast), allows to study storm surge's by measuring the Total Water Level Envelope (TWLE), and it is also very useful in wave models. However, coastal altimetry data is inaccurate and difficult to interpret due to the variation of the waveforms' shape (shape of the radar returns), when the antenna footprint of the instrument enters in the land, and because of the rapid variations of the wet tropospheric delay. The application of SAR techniques to radar altimetry, such as in ESA's CryoSat-2 mission has allowed to significantly improve the along-track resolution, providing much better results than in pulse-limited altimeters. Nevertheless for these high-resolution altimeters, an optimized delay correction is needed to solve the rapid tropospheric wet delay variability [1].

In this study a methodology is presented to identify from the measured brightness temperature of the atmosphere, a set of frequency channels that provide the most significant and uncorrelated information on the water vapor content in the atmosphere. Previous works [2] have provided a water vapor content analysis based on the number of degrees of freedom for a ground-based zenith-viewing model, assuming clear skies, and different seasons. A similar brightness temperature model, based on space-based observations is presented in this study. However, unlike in [2], in this work, the water vapor entropy is used to define the optimum channels, for three different climates and types of surfaces.

First of all a Mathematical model is defined to describe the Physics of the atmosphere, and from this model the contribution of the water vapor into the brightness temperatures as measured by a nadir-looking microwave radiometer are derived. Then, a Mathematical model using inversion methods to select frequency channels providing the largest amount of data (i.e. uncorrelated data) is defined. Finally, results for three "standard" climates (tropical, temperate, and polar) are presented. Synthetic atmospheric pressure, temperature, and water vapor profiles are used, and different surface emissivities are also considered in the computation of the down-looking brightness temperatures for the three atmosphere models.

II. METHODOLOGY

A. Forward Model

In this study three different atmosphere models are considered for the three different climates: tropical, temperate, and polar, and for the three different types of surfaces: ice, sea, and coastal regions. The three standard atmosphere models are generated using as input parameters the water vapor, temperature, and pressure from 0 km (sea surface height), up to 64 km height (mesosphere). The atmospheric temperature, pressure, and water vapor profiles (T(z), P(z), and $\rho_v(z)$) for the three different climates are described in [3, pp. 339-373] (Fig. 1), and they are used to compute the gas absorption ($\kappa_\alpha(f,z)$) as a function of the frequency and height, the atmospheric optical thickness ($\tau(z,\infty)$), the upwelling temperature (T_{UP}), and down-welling temperature (T_{DN}) as a function of the frequency (f). Finally, three different surface emissivities are used to calculate the surface brightness temperature (T_b), and the downwelling temperature reflected back to the atmosphere (T_{sc}).

The emissivity values are 1.00, 0.50 and 0.75, which correspond approximately to those of the ice, ocean, and coastal regions, respectively. Finally, the brightness temperature reaching the radiometer antenna (T_B, Eqn. 1) is then computed for the nine possible combinations of the three different climates and the three different surfaces:

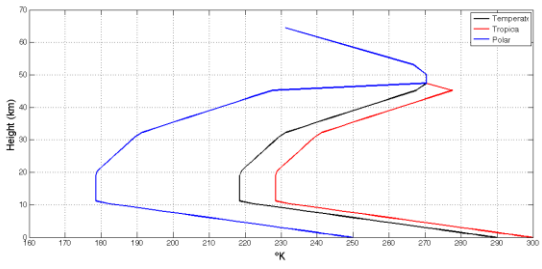

a)

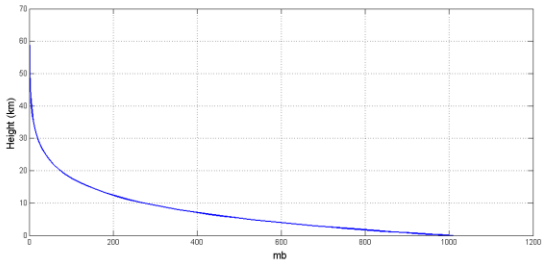

b)

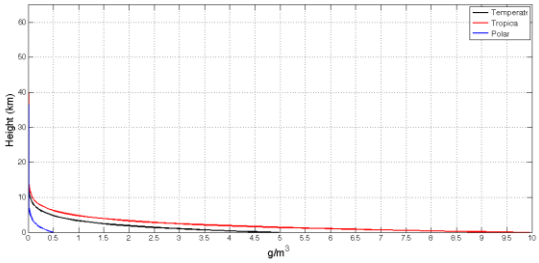

c)

Fig. 1. Atmospheric temperature, pressure, and water vapor profiles used for the three climate models.

$$T_B = T_{UP} + (T_b + T_{SC}) \cdot e^{-\tau(0,\infty)}, \quad (1)$$

$$T_{UP} = \sec(\theta) \cdot \int_0^\infty \kappa_\alpha(f,z) \cdot T(z) \cdot e^{-\tau(z,\infty)} \cdot dz, \quad (2)$$

$$T_b = e_s \cdot T_s \cdot e^{-\tau(0,\infty)}, \quad (3)$$

and

$$T_{SC} = (1 - e_s) \cdot \sec(\theta) \cdot \int_\infty^0 \kappa_\alpha(f,z) \cdot T(z) \cdot e^{-\tau(0,z)} dz, \quad (4)$$

where each contribution to the brightness temperature is represented in the Fig. 2. In Eqns. 3 and 4, e_s and T_s are the surface's emissivity and temperature, and θ is the zenith angle.

The brightness temperature reaching the radiometer (T_B) can also be written as:

$$T_B = \sec(\theta) \cdot \int_0^\infty \rho_v(f,z) \cdot K^{\uparrow}{}_W(f,\theta,z) \cdot dz, \quad (5)$$

where $K^{\uparrow}{}_W$ is the so-called water vapor weighting function, which indicates the contribution of the atmospheric water vapor content at height z, to the measured brightness temperature (T_B) at a frequency f, under an observation angle θ (θ = 0° at nadir) and, over surface with emissivity e_s [4]. The water vapor weighting function is calculated as the derivative of the brightness temperature with respect to the water vapor profile:

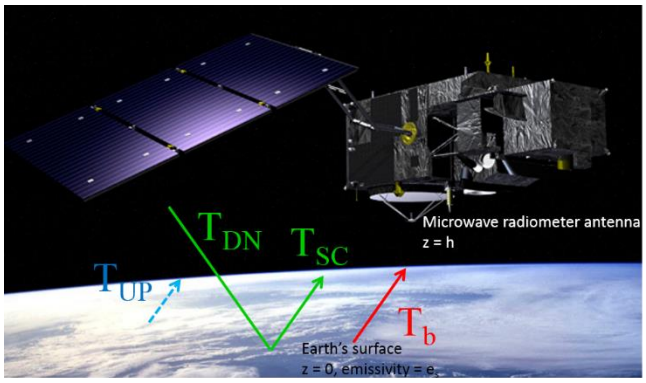

Fig. 2. Schematic observation brightness temperatures.

$$K^{\uparrow}{}_W(f,\theta,z) = \frac{\partial \kappa_\alpha(f,T,\rho_v)}{\partial \rho_v} \cdot \sec(\theta) \cdot e^{-\tau(z,h)} \cdot \left\{ -[(1-\epsilon) \cdot T_{DN} + \epsilon \cdot T_s] \cdot e^{-\tau(0,z)} - \int_0^z T(z') \cdot \kappa_\alpha(f,T,\rho_v) \cdot \sec(\theta) \cdot e^{-\tau(z',z)} dz' \right\} + K^{\downarrow}{}_W(f,\theta,z), \quad (6)$$

where $K^{\downarrow}{}_W(f,\theta,z)$ is the water vapor weighting function for an upward looking radiometer:

$$K^{\downarrow}{}_W(f,\theta,z) = \frac{\partial \kappa_\alpha(f,T,\rho_v)}{\partial \rho_v} \cdot \sec(\theta) \cdot e^{-\tau(h,z)} \cdot \left\{ -\int_z^h T(z') \cdot \kappa_\alpha(f,T,\rho_v) \cdot \sec(\theta) \cdot e^{-\tau(z,z')} dz' \right\}. \quad (7)$$

Equation 6 allows to analyze the sensibility of the observation (i.e. frequency channel) to the atmospheric water vapor variations, and the impact of different surfaces (ice, ocean, and coastal) can be evaluated.

B. Channel selection based on the amount of information content

The methodology used in this study consists of the analysis of the sensibility to the atmospheric water vapor content of the brightness temperatures measured from the space by a down-looking microwave radiometer, and the evaluation of the optimum set of frequency channels that provides the largest amount of information on the water vapor content, i.e. the information provided by the selected channels is most uncorrelated. Once a channel is selected, the information provided is considered to be known at the time to select further channels, i.e. it is no longer a variable, avoiding redundant data.

B.1 Information content

To compute the information content of the different frequency channels, the concept of entropy of the probability density functions is used as defined by Shannon in Information Theory [5, pp. 33-34]. The quantity of information of a given parameter that is provided by some observations (frequency channel) is computed as the change in the information entropy from a prior knowledge state of this parameter, and its knowledge after that observation. This is expressed in Eqns. 8 and 9, where the analyzed state is x, the observations are y, S indicates the entropy of the state with

probability P, and H is the reduction in the entropy or information content.

$$H_n = S[P(\boldsymbol{x})] - S[P(\boldsymbol{x}|\hat{\boldsymbol{y}})]\,, \tag{8}$$

$$H_m = S[P(\hat{\boldsymbol{y}})] - S[P(\hat{\boldsymbol{y}}|\boldsymbol{x})]. \tag{9}$$

In Eqn. 8 the entropy reduction is evaluated in the state space or atmospheric profile, i.e. the change in the entropy of the state vector when it is improved by the measurements, where the subscript n is the number of atmospheric layers. In Eqn. 9 the entropy reduction is evaluated in the measurement space, i.e. the change in the entropy of the measurements when the state space is previously known, where the subscript m is the number of observation channels (or frequencies). The result obtained for each equation is the same, and could be combined to measure the reduction entropy when other channels are previously selected.

B.2. Model linearization

The forward model presented in Eqns. 1 and 5 can be discretized in order to facilitate the calculation using algebraic methods [4]. This discrete model is presented below, where the bold symbols indicate vectors (lower case) and matrices (upper case).

$$\hat{\boldsymbol{y}} = \boldsymbol{K_W} \cdot \boldsymbol{x} + \boldsymbol{\varepsilon}. \tag{10}$$

In this discrete model the brightness temperature observations are represented by the vector $\hat{\boldsymbol{y}}$, whose dimension corresponds to the number of observation channels (frequency channels) to be analyzed. The unknown profile information along the atmospheric height z is $\boldsymbol{x}$, the error of each observation caused by the instruments' calibration and the noise is $\boldsymbol{\varepsilon}$, and the contribution of each atmospheric profile component per height and frequency to the brightness temperature is given by the matrix $\boldsymbol{K_W}$. The weighting function matrix $\boldsymbol{K_W}$ is m x$_n$, where there is a contribution to the brightness temperature at each frequency channel (m channels) from each layer (n layers). The number of layers (n) is 60 between 0 and 64 km in steps of 0.1 to 0.8 km for the troposphere, 0.8 to 2 km for the stratosphere and, 2 to 4 km for the mesosphere. The total number of channels (m) around the water vapor resonance frequencies (22.235 GHz and 183.3 GHz) are analyzed in steps of 100 MHz.

The probability density function of the measurements is assumed to be Gaussian function in order to use its properties, and to relate the probability density function of the observations with the one of the atmospheric state (Eqns. 8 and 9), by using Bayes' theorem (Eqns. 11 and 12).

$$P(\hat{\boldsymbol{y}}|\boldsymbol{x}) = P(\boldsymbol{x},\boldsymbol{y})/\textstyle\int P(\boldsymbol{x},\hat{\boldsymbol{y}}), \tag{11}$$

$$P(\boldsymbol{x}|\boldsymbol{y}) = P(\hat{\boldsymbol{y}}|\boldsymbol{x}) \cdot P(\boldsymbol{x})/P(\hat{\boldsymbol{y}}). \tag{12}$$

Assuming $P(\hat{\boldsymbol{y}})$ and $P(\boldsymbol{x})$ are Gaussian functions with a zero-mean experimental error $\boldsymbol{\varepsilon}$, Eqns. 11 and 12 become:

$$P(\boldsymbol{y}) = \frac{1}{(2\pi)^{\frac{n}{2}} \cdot |\boldsymbol{S_y}|^{\frac{1}{2}}} \cdot e^{-\frac{1}{2}\cdot(\boldsymbol{y}-\boldsymbol{E(y)})\cdot\boldsymbol{S_y^{-1}}\cdot(\boldsymbol{y}-\boldsymbol{E(y)})}\,, \tag{13}$$

$$P(\boldsymbol{x}) = \frac{1}{(2\pi)^{\frac{n}{2}} \cdot |\boldsymbol{S_a}|^{\frac{1}{2}}} \cdot e^{-\frac{1}{2}\cdot(\boldsymbol{x}-\boldsymbol{x_a})\cdot\boldsymbol{S_a^{-1}}\cdot(\boldsymbol{x}-\boldsymbol{x_a})}, \tag{14}$$

where the matrices $\boldsymbol{S_y}$ and $\boldsymbol{S_a}$ are the covariance matrices of $\hat{\boldsymbol{y}}$ and $\boldsymbol{x_a}$, respectively, and the subscript a denotes the *a priori* knowledge coming from historical information of the atmosphere or from synthetic data as in the case of this study. By combining Eqns. 13 and 14 [5, pp. 23 – 29], the covariance matrix of the state vector improved by the brightness temperature observations (Eqn. 12) can be written as:

$$\hat{\boldsymbol{S}}^{-1} = \boldsymbol{K_W^T} \cdot \boldsymbol{S_\varepsilon^{-1}} \cdot \boldsymbol{K_W} + \boldsymbol{S_a^{-1}}. \tag{15}$$

From the discretization of the observations and the atmospheric state given by Eqn. 10, and defining the relationship between the *a priori* knowledge of the atmospheric state $\boldsymbol{x}$ with the knowledge gain obtained through the observations (Eqns. 11 and 12), the recovered state vector $\hat{\boldsymbol{x}}$ can be expressed as:

$$\hat{\boldsymbol{x}} = \boldsymbol{x_a} + \boldsymbol{S_a} \cdot \boldsymbol{K_W^T} \cdot \left(\boldsymbol{K_W} \cdot \boldsymbol{S_a} \cdot \boldsymbol{K_W^T} + \boldsymbol{S_\varepsilon}\right)^{-1} \cdot (\hat{\boldsymbol{y}} - \boldsymbol{K_W} \cdot \boldsymbol{x_a}), \tag{16}$$

that can also be rewritten as:

$$\hat{\boldsymbol{x}} = \boldsymbol{x_a} + \boldsymbol{G} \cdot (\hat{\boldsymbol{y}} - \boldsymbol{K_W} \cdot \boldsymbol{x_a}), \tag{17}$$

where $\boldsymbol{G}$ denotes the contribution matrix or gain matrix. The so-called Averaging Kernel (Eqn. 18):

$$\boldsymbol{AK} = \boldsymbol{S_a} \cdot \boldsymbol{K_W^T} \cdot \left(\boldsymbol{K_W} \cdot \boldsymbol{S_a} \cdot \boldsymbol{K_W^T} + \boldsymbol{S_\varepsilon}\right)^{-1} \cdot \boldsymbol{K_W} \cdot \boldsymbol{S_a} \tag{18}$$

describes the vertical correlation between the parameters at different heights for a given set of frequency channels, and it will be used to measure the entropy reduction by each channel.

B.3. Channel Selection Iterative Method

The method used to select the optimum set of frequencies consists of the evaluation of the information content of each individual frequency channel, and taking into account the previously selected ones (Eqns. 8 and 9). The change on the measurement entropy caused by each selected channel is evaluated (Eqn. 9), which at the same time changes the vertical entropy (Eqn. 8). From the linearized model of the previous section (Eqn. 10), the entropy (in bits) of a multivariate Gaussian distribution for a vector can be approximated as:

$$S[P(\boldsymbol{y})] \approx \tfrac{1}{2}\log_2[S(\boldsymbol{y})], \tag{19}$$

where $S(\boldsymbol{y})$ is the covariance matrix of this vector. Thus, for the discrete model in Eqn. 9 can be expressed as:

$$H_m = \tfrac{1}{2}\log_2\left[\boldsymbol{I_m} + \boldsymbol{K'_W} \cdot \boldsymbol{A} \cdot \boldsymbol{K'^T_W}\right], \tag{20}$$

where

$$\boldsymbol{K'_W} = \widehat{\boldsymbol{S_\varepsilon}}^{-\frac{1}{2}} \cdot \boldsymbol{K_W}\,, \tag{21}$$

and $\boldsymbol{A}$ indicates the improvement of the different frequencies on the atmospheric profile information or state vector [5, pp. 29 – 33], [6].

From Eqns. 8 and 18, the entropy reduction in the state space can be evaluated as:

$$H_n = -\frac{1}{2}\cdot \log_2[\boldsymbol{I_n} - \boldsymbol{S_a}\cdot \boldsymbol{K_W^T}\cdot \left(\boldsymbol{K_W}\cdot \boldsymbol{S_a}\cdot \boldsymbol{K_W^T} + \boldsymbol{S_\varepsilon}\right)^{-1}\cdot \boldsymbol{K_W}]. \quad (22)$$

and from Eqn. 18, it can be expressed as:

$$H_n = -\frac{1}{2}\cdot \log_2[\boldsymbol{I_n} - \boldsymbol{AK}]. \quad (23)$$

The change in the state space covariance because of the selected channels is:

$$\boldsymbol{A} = \left[\boldsymbol{I_n} - \boldsymbol{S_a}\cdot \boldsymbol{K_W^T}\cdot \left(\boldsymbol{K_W}\cdot \boldsymbol{S_a}\cdot \boldsymbol{K_W^T} + \boldsymbol{S_\varepsilon}\right)^{-1}\cdot \boldsymbol{K_W}\right]\cdot \boldsymbol{S_a}, \quad (24)$$

and from Eqn. 22:

$$-\frac{1}{2}\cdot \log_2[\boldsymbol{A}] = H_n + \log_2[\boldsymbol{S_a}]. \quad (25)$$

Finally, Eqn. 20 can be expressed as the entropy in the measurement space of the remaining channels updated by the entropy in the state space for the selected channels:

$$H_m = \frac{1}{2}\log_2\left[\boldsymbol{I_m} + \boldsymbol{K'_W}\cdot H_n \cdot \boldsymbol{S_a}\cdot \boldsymbol{K'^T_W}\right], \quad (26)$$

Using Eqn. 26 iteratively, the information content of channel i (Entropy Reduction or δER_i) can be evaluated separately (Eqn. 27). The one providing the largest amount of information is then kept:

$$\delta ER_i = \frac{1}{2}\log_2[1 + \boldsymbol{k'}_{\boldsymbol{w_i}}\cdot \boldsymbol{A_{i-1}}\cdot \boldsymbol{k'^T}], \quad (27)$$

where $\boldsymbol{A_{i-1}}$ accounts for the channels previously selected.

$$\boldsymbol{A_i} = \boldsymbol{A_{i-1}} - \frac{(\boldsymbol{A_{i-1}}\cdot \boldsymbol{k_i}'^T)\cdot(\boldsymbol{A_{i-1}}\cdot \boldsymbol{k_i}'^T)^T}{1+(\boldsymbol{A_{i-1}}\cdot \boldsymbol{k_i}'^T)^T\cdot \boldsymbol{k_i}'^T}, \quad (28)$$

with $\boldsymbol{A_0} \triangleq \boldsymbol{S_a}$.

III. WATER VAPOR RESONANCE FREQUENCIES

The Entropy Reduction method gives a ranking of the most suitable frequencies (channels) to retrieve the atmospheric component of interest, from a spaceborne radiometer. Furthermore, the frequencies are evaluated by considering their contribution in case a set of channels is used for the analysis, i.e. the information provided by a frequency (channel) is uncorrelated to the one provided by the previously selected channels, in case there is a previous selection iteration. As explained in section 2, the information content of each frequency is measured through the water vapor weighting functions from the down-looking brightness temperature (Eqn. 6), which provides the sensibility of the measured brightness to changes in the atmospheric water vapor profile. This sensibility is evaluated considering the radiation emitted by the atmosphere directly to the downlooking spaceborne radiometer (T_{UP}), the radiation emitted by the atmosphere down to the surface (T_{SC}) and reflected back to the space radiometer (T_{DN}), and the radiation emitted by the Earth surface (T_B). The atmospheric radiation emitted to the space, gives the trend of the water vapor with regards to the climate, however, it does not provide information on the impact of the surface change on the variability of the atmospheric water vapor content. Water vapor profile changes caused by the surface characteristics, are a case of interest for this study to correct the electrical path wet delay on coastal altimeters, as its rapid variability is one of the main reasons that makes this information inaccurate. The information on the effect of the surface into the atmospheric state is given by the reflected downwelling temperature, and by the surface emitted temperature, which are directly related to the surface emissivity.

Temperate and tropical climates are wetter than polar climate, which is practically dry. It causes that around the water vapor absorption window around 183.31 GHz, the oblique transmissivity for temperate and tropical climates is zero (opaque atmosphere), while in polar climates is between 20-30%. This fact affects to the depth along the atmosphere to which the radiometers can measure the water vapor content in temperate and tropical climates, making frequencies around 183.3 GHz not suitable for surface water vapor variability studies, being necessary to move to the tails of this resonance frequency to better analyze the sensitivity to the water vapor [7, pp. 1-9]. On the other hand, in the low water vapor absorption window, around 22.23 GHz, the oblique transmissivity is higher for the three climates (ratio between 85-95% in tropical and temperate climates, and ~100% in polar climates), making it possible to analyze the surface emissivity effects on the water vapor variability of the low-troposphere. On the other hand, due to the fact that the water absorption lines are stronger at the higher resonance frequencies (183.31 GHz), the information content provided in these frequencies would be always larger than the one provided by the lower frequencies (22.23 GHz). However, the information content measured in the 183.31 GHz window in temperate and tropical climates will be coming from the mid-low troposphere. Therefore it is necessary to analyze both absorption windows separately, and from the two remaining set of frequencies, select those ones that include information along all the mid-lower troposphere.

IV. SIMULATION RESULTS

In a preliminary study all the frequency channels from 1 to 200 GHz were studied, considering only the contribution of the atmospheric water vapor to the upwelling brightness temperature (T_{UP}). Results confirmed the intuition, that the best bands are around the lower (~22 GHz), and higher (~183 GHz) water vapor resonance frequencies. Therefore, only the meaningful results for these frequency bands are presented here.

Figures 3 and 4 show the application of the iterative method to the different resonance frequencies, that is the δER_i for the channels that provide the largest amount of information. This is done for the three climates: temperate, tropical and polar, and for the three surfaces: sea, coast, and ice. In these figures, the first iteration of the method (when the first channel is selected) is shown, and then the following iterations, until a significant number of bits of information it is retained, that in this study the threshold is above 0.2 bits of information. Figure 3shows the δER_i for the low (~22 GHz) band and for three different surface emissivities. As mentioned in the previous section, resonance frequencies do not turn to be the optimum ones to retrieve information about the state of the atmosphere, as they are strongly affected by the attenuation. In these figures it can be observed that the trend of the information provided does not vary, that means that the optimum frequencies do not change. However, for increasing surface emissivity (from sea e_s~0.50 to ice e_s~1.00), the information provided by the optimum frequencies also increases. It means that the information

given by the surface temperature emitted to the space contains more information about the water vapor distribution in the atmosphere than the reflected downwelling temperature. This is due to the fact that as the upwelling temperature, the downwelling temperature corresponds to the radiation emitted by the atmosphere, so it is expected that the information provided is somewhat similar to the one provided by the upwelling temperature. In other words, the information is correlated. At lower frequencies, the information provided by the main channels decays rapidly, i.e. one channel provides almost all the information. This fact indicates that the water vapor information provided by the lowest frequency channels is less impacted by the atmosphere gas absorption which is highly correlated, and practically one channel provides most of the information.

Higher resonant frequencies (Fig. 4) provide actually the largest amount of information on the water vapor for the three climates analyzed. In all cases, the main channels correspond to the three first channels of the highest frequencies. As in case of the lowest resonance frequencies, the tails of the sounding channels are best suited to obtain more information, as there is less affectation of the gas absorption.

At both high and low resonance frequencies, the distribution of the information between the remaining channels has a common behavior when a channel is selected. Each time a channel is selected, the information of the remaining channels is reevaluated, discarding those channels that provide information correlated to the information already provided with the selected ones. Since the main channels are at the tails of the resonance frequencies, it can be observed that after the 3th or 4th iteration, the channels containing most information start getting closer to the resonant frequencies. This indicates that the tails are less attenuated, but more correlated among them in terms of amount of information. This effect is clearly visible for the high resonance frequencies in tropical climates. Tables 1–3 show in detail these results numerically.

Finally, Fig. 5 presents the weighting functions for the main frequency channels of each climate and surface emissivity. As it can be seen, the first four channels contain information on the water vapor in the troposphere up to ~5-7 km for temperate and tropical climates, and up to ~3-4 km for polar climates. These figures give also a clear view of the impact of the surface emissivity on the sensibility of the brightness temperature to the atmospheric water vapor. As previously discussed, the increase of the surface emissivity augments the presence of the surface temperature into the observations that contains important information on the variability of the water vapor in lower layers of the troposphere, and it is more uncorrelated to the upwelling brightness temperature than the reflected downwelling brightness temperature. This effect can be observed through the polar climates, where there is lower concentration of water vapor in the troposphere. In Figs. 5g-h it can be observed that a frequency channel at 183.4 GHz provides the largest information from the lower troposphere when the surface emissivity is increased. This fact enhances the presence of the surface temperature (T_b) into the retrieved brightness temperature (T_B), that as explained previously is less correlated with the atmospheric radiated temperatures (T_{DN}, and T_{UP}), so that provides more information about the water vapor distribution.

V. CONCLUSIONS AND FUTURE RESEARCH LINES

Most sea surface altimetry missions make use of two or three frequency bands. For example, the radiometer onboard Saral is included in the AltiKa instrument and it is a dual-frequency channel microwave radiometer (23.8 and 37 GHz) to provide information related to the water vapor content and the cloud liquid water content. The Jason-3 radiometer is a three channel microwave radiometer: the 23.8 GHz channel is the primary water vapor sensor, the 34 GHz channel provides a correction for non-raining clouds, and the 18.7 GHz channel provides the correction for effects of wind-induced enhancements in the sea surface background emission. On the other hand, other water vapor radiometers, as BEST, are also two channels radiometers, but centered at 150 GHz, and 165 GHz..

However, in this study, it has been found that up to four frequency channels may be worth using, since they convey the largest amount of information for all three climates, and information provided by further channels provide at least 4 bits less of information than the previous selected ones. In high resonance frequencies, the channels that provide the most information are 175.1 GHz, ~188.1 GHz, and ~185.5 GHz for temperate climates, 175.1 GHz, ~188.5 GHz, and ~186.3 GHz for tropical climates and ~185.5 GHz, 189.2 GHz, and 183.5 GHz for polar climates, while in lower absorption bands the optimum channels are: 22.7 GHz, and 25.5 GHz for the temperate climates, 22.7 GHz, and 26 GHz, and around 30 GHz for polar climates. These frequency channels are quite similar for tropical and temperate climates, but differ from those at polar climates. The number of channels to be included in a radiometer instrument will be ultimately dictated by: 1) the achievable accuracy of the water vapor correction for a given number of frequency channels and associated radiometric errors (both radiometric accuracy or systematic errors, and radiometric sensitivity of random errors), and 2) the instrument complexity and cost, which increases with the number of channels.

On the other hand, channels of the lowest resonance frequencies which are more sensitive to changes in the surface's emissivity must be included, as they are very sensitive to the variability of water vapor in coastal zones.

However, a much better spatial resolution can be achieved using the highest frequency channels, as compared to the low frequency channels, for the same antenna size. The use of the resonance frequencies provides less accurate information about the troposphere, due to the higher absorption by the water vapor.

Future research lines of this study will extend the range of frequencies (f>200GHz), will consider the atmospheric scattering by hydrometeors, and will perform a study of the achievable wet delay retrieval accuracy as a function of the number of channels and their radiometric errors.

Table 1. Entropy reduction for low and high frequency channels: temperate climate.

Surface's emissivity e_s=0.50		Surface's emissivity e_s=0.75		Surface's emissivity e_s=1.00	
f [GHz]	**ER [bits]**	**f [GHz]**	**ER [bits]**	**f [GHz]**	**ER [bits]**
22.7	6.001	22.7	6.498	22.7	6.868
25.5	1.220	25.6	1.550	25.6	1.824
22.4	0.486	22.4	0.503	22.4	0.513
25.6	0.429	25.5	0.456	25.5	0.471
22.5	0.286	22.3	0.292	22.3	0.296
25.7	0.267	25.7	0.277	25.7	0.282
22.3	0.204	22.5	0.207	22.5	0.208
175.3	9.700	175.1	9.769	175.1	9.837
187.4	7.349	187.5	7.405	187.5	7.437
185.4	5.672	185.5	5.735	185.5	5.751
189.4	3.952	189.6	3.964	189.6	4.050
184.1	3.435	184.1	3.531	184.1	3.535
183.4	1.054	184.8	1.158	184.8	1.162
186.2	0.935	183.4	0.877	183.4	0.877

Table 2. Entropy reduction for low and high frequency channels: tropical climate.

Surface's emissivity e_s=0.50		Surface's emissivity e_s=0.75		Surface's emissivity e_s=1.00	
f [GHz]	**ER [bits]**	**f [GHz]**	**ER [bits]**	**f [GHz]**	**ER [bits]**
22.7	7.957	22.7	8.395	22.8	8.732
26.0	3.474	26.0	3.858	26.0	4.115
24.1	0.618	24.0	0.716	24.0	0.779
30.0	0.567	30.0	0.639	30.0	0.704
22.3	0.526	22.3	0.537	22.3	0.595
24.2	0.326	24.2	0.351	24.2	0.361
29.9	0.312	29.9	0.331	29.9	0.344
175.1	10.480	175.1	10.496	175.1	10.511
188.5	8.158	188.6	8.166	188.6	8.174
186.2	6.573	186.3	6.607	186.3	6.611
184.8	4.993	184.9	5.069	184.9	5.071
176.8	4.609	176.7	4.489	176.7	4.544
183.9	3.037	183.9	3.177	183.9	3.179
187.2	1.937	187.2	1.823	187.2	1.838

Table 3. Entropy reduction for low and high frequency channels: polar climate.

Surface's emissivity e_s=0.50		Surface's emissivity e_s=0.75		Surface's emissivity e_s=1.00	
f [GHz]	**ER [bits]**	**f [GHz]**	**ER [bits]**	**f [GHz]**	**ER [bits]**
30.0	1.047	30.0	1.491	30.0	1.844
29.9	0.405	29.9	0.448	29.9	0.467
29.8	0.255	29.8	0.271	29.8	0.278
185.4	5.670	185.6	5.787	185.9	5.905
188.7	2.198	189.2	2.366	183.5	2.631
183.4	1.190	183.4	1.315	189.8	1.258

REFERENCES

[1] S. Vignudelli, A. Kostianoy, P. Cipollini, and J. Benveniste, Coastal Altimetry, *Springer-Verlag Berlin Heidelberg*, 2011.

[2] S. Sahoo, X. Bosch-Lluis, S. C. Reising and J. Vivekanandan, "Radiometric Information Content for Water Vapor and Temperature Profiling in Clear Skies Between 10 and 200 GHz," in IEEE Journal of Selected Topics in Applied Earth Observations and Remote Sensing, Vol. 8, No. 2, pp. 859-871, Feb. 2015.

[3] F. T. Ulaby and D. G Long, *Microwave Radar and Radiometric Remote Sensing*. USA: The University of Michigan Press, ch. 8-9, pp. 326-373, December, 2013

[4] M. Klein, and A. J. Gasiewski "Nadir sensitivity of passive millimeter and submillimeter wave channels to clear air temperature and water vapor variations", *Journal of Geophysical Research,* vol. 105, no. D13, pp. 17481 – 17511, July, 2000. doi:10.1029/2000JD900089.

[5] C. D. Rodgers, *Inverse Methods for atmospheric remote sounding: Theory and Practice*, USA: World Scientific Publishing Co. Pte. Ldt., ch. 2, pp. 20 – 37.

[6] F. Rabier, N. Fourrié, D. Chafäi, and P. Prunet, "Channel selection methods for Infrared Atmospheric Sounding Interferometer radiances", *Q. J. R. Meteorol. Soc*, vol. 128, pp. 1011 – 1027, September, 2001. doi:10.1256/0035900021643638

[7] Lee-Lueng Fu, and A. Cazenave, Satellite Altimetry and Earth Sciences, Vol. 69, 1st Edition, A Handbook of Techniques and Applications, ch. 2, pp. 4 – 11, ed. Elsevier, 2000.

AKNOWLEDGEMENTS

This project has received funding by the Spanish Ministry of Economy and Competitiveness ESP2015-70014-C2-1-R (MINECO/FEDER).

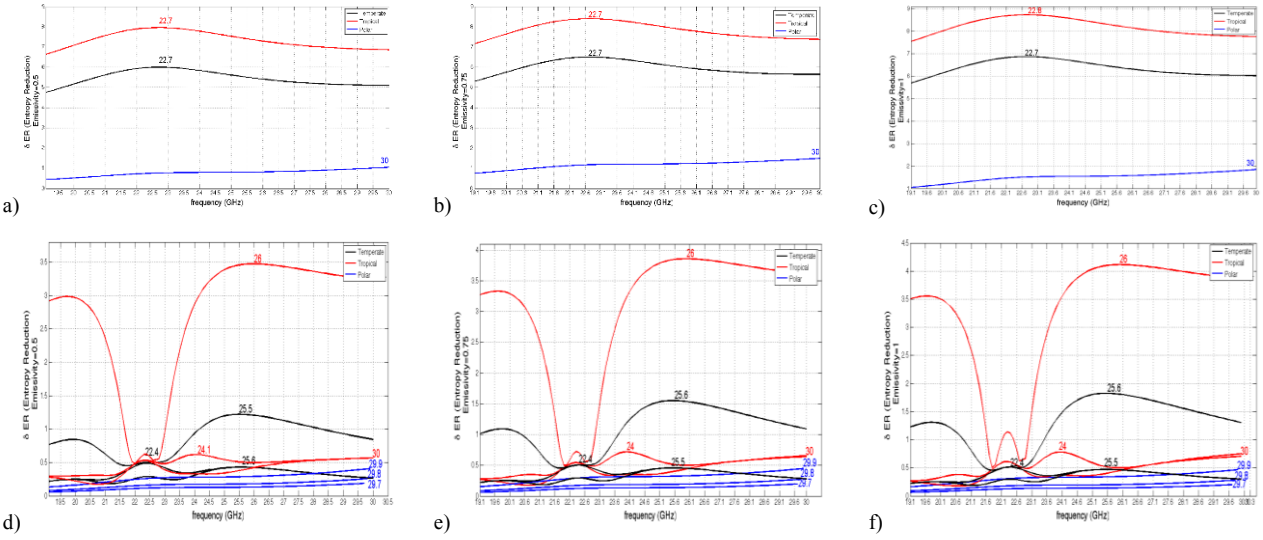

Fig. 3. Entropy Reduction for low frequency channels, for different climates (black: temperate, red: tropical, blue: polar), and different surface emissivities (a-d: e_s=0.50; b-e: e_s=0.75, e_s=1.00). Top row: Entropy reduction when fist channel is selected. Bottom row: Entropy reduction when second, third and fourth channels are selected.

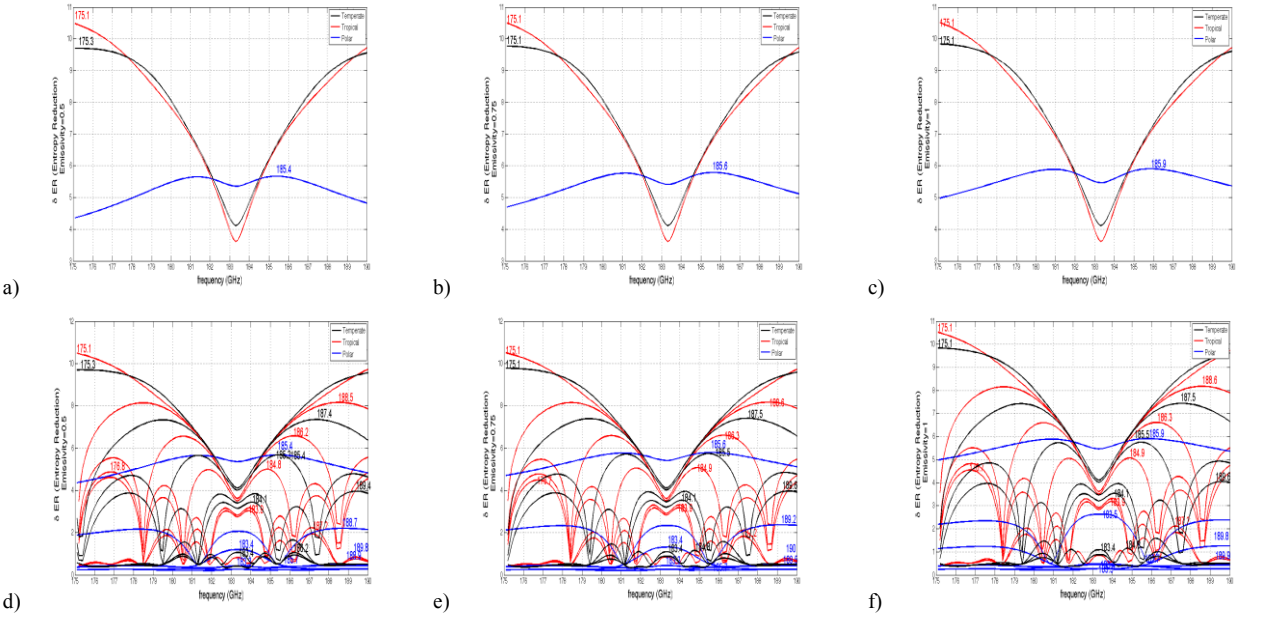

Fig. 4. Entropy Reduction for high frequency channels, for different climates (black: temperate, red: tropical, blue: polar), and different surface emissivities (a-d: e_s=0.50; b-e: e_s=0.75, e_s=1.00). Top row: Entropy reduction when fist channel is selected. Bottom row: Entropy reduction when second to sixth channels are selected.

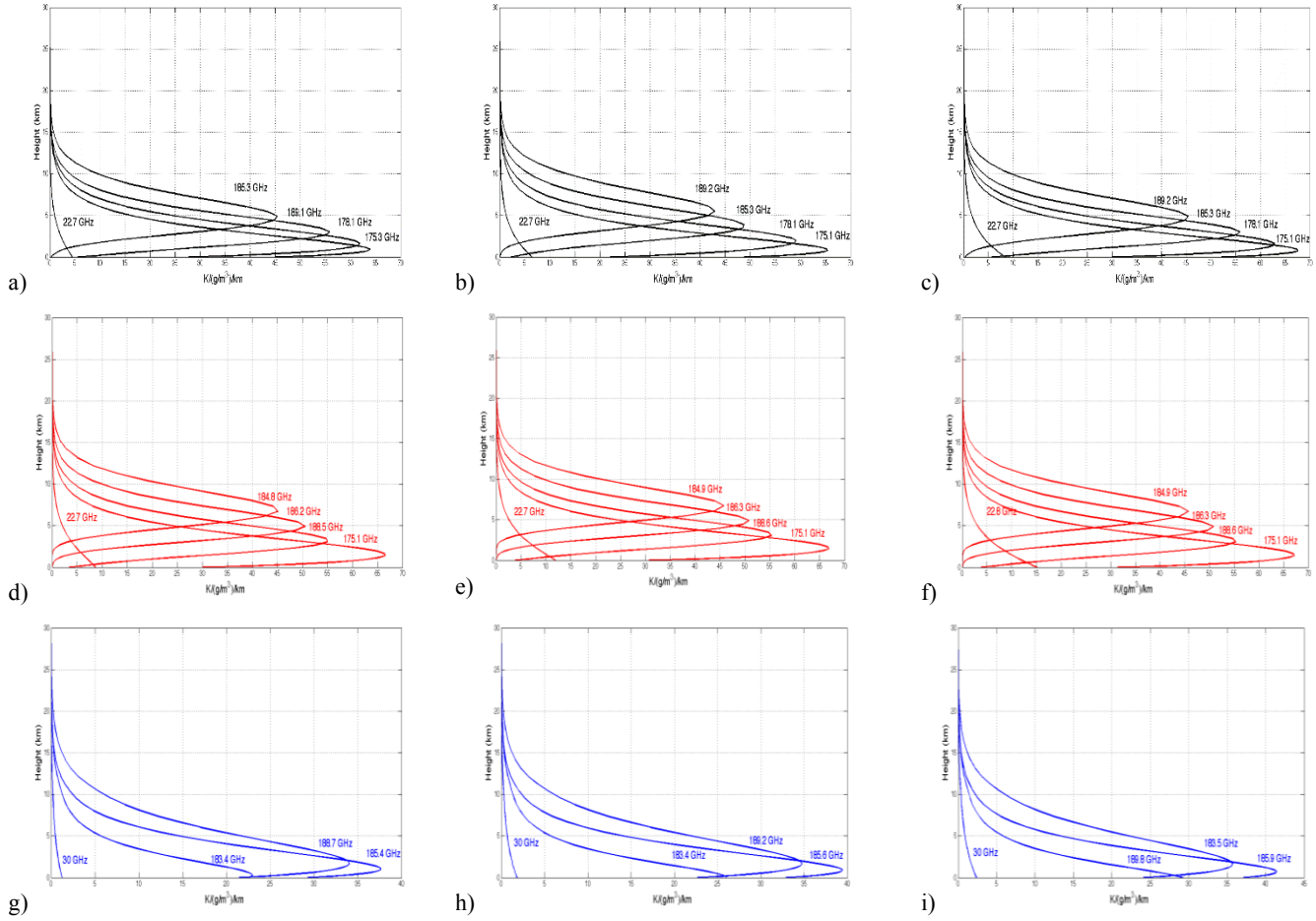

Fig. 5. Weighting functions for: a-b-c) temperate, d-e-f) tropical, and g-h-i) polar climates for the least correlated frequency channels over different surface emissivities: a-d-g) es=0.50; b-e-h) es=0.75; and c-f-i) es=1.00.